Compression Load Failure of Aluminum Plates due to Fire

Emily J. Fogle[1], Brian Y. Lattimer[1*], Stefanie Feih[2], Everson Kandare[2], Adrian P. Mouritz[2], and Scott W. Case[3]

[1]Department of Mechanical Engineering, Virginia Tech, Blacksburg, VA USA
[2]School of Aerospace, Mechanical & Manufacturing Engineering, RMIT University, Australia
[3]Department of Engineering Science & Mechanics, Virginia Tech, Blacksburg, VA USA

Engineering Structures Journal

* Corresponding Author: Dr. B.Y. Lattimer
e-mail: lattimer@vt.edu
tel: +1 540 231 7295
fax: + 1 540 231 9100
address : Virginia Polytechnic Institute and State University
Department of Mechanical Engineering
203 Randolph Hall (MC 0238)
Blacksburg, VA 24061 USA

ABSTRACT

An experimental study was performed to quantify the response and failure of 5083-H116 and 6082-T6 aluminum plates under compression load while being subjected to a constant heat flux representing a fire exposure. Using an intermediate scale loading frame with integrated heating, the study evaluated the effects of geometry, aluminum type, fire exposure, load, and fire protection. Intermediate scale aluminum panels which were more than 0.7 m high and 0.2 m wide were used to gain insights into the structural behavior of large structural sections exposed to fire. Failure temperatures were measured to range from 100-480^{o}C and were dependent on applied stress and aluminum type. This indicates that the use of a single temperature criterion in fire resistance without load as typically done is not sufficient for evaluating structural response during fire. An empirical failure model was developed to account for fire exposure conditions, aluminum type, and geometry.

KEYWORDS : aluminum, fire, compression, failure

INTRODUCTION

Corrosion resistant aluminum is being considered for a variety of structural applications such as bridge decks, marine crafts, and off-shore platforms. Some of these aluminum structures are required to meet fire resistance requirements, which include the structural response of the material during fire. The structural response of aluminum during fire has not been well studied and still relies primarily on large-scale testing to design for fire. The focus of this study is on the response of aluminum during compression loading.

Studies have been reported on the structural response of aluminum under compression at room temperature for flat plates [1], different cross-sections [2-4], and effects of welds [1,3,4]. Elevated temperature thermo-structural response of aluminum alloys under compression loading has been measured for columns and sections with welds [6-8]. These studies used intermediate-scale components to evaluate response. Failure temperatures were measured to range from 170-350^{o}C for 5xxx and 6xxx series aluminum [6-10]. Experiments were performed with constant temperature [6] or linear ramping of temperature (2-11^{o}C/min) [6-10], which is not consistent with realistic fire exposures.

Select studies have investigated the performance during more realistic fire exposures such as standard fire resistance tests and constant heat flux exposures. Structural response during large-scale fire resistance tests have been reported on bulkheads [12] and aluminum columns including the effects different cross-sections and fire protection [11,19]. Failure temperatures in large scale fire resistance tests, which ranged from 250-450^{o}C, were related to the applied stresses [11]. Large-scale tests did not evaluate the effects of exposure severity. Small-scale tests (0.05-0.1 m samples) were performed to investigate the effects of exposure level and load [13,14]. Failure temperatures were reported to vary between 130-360^{o}C for applied stresses ranging from 20-80% of the room temperature buckling load [14]. The small-scale tests, however, may not be reflective of larger scale response due to failure modes and boundary condition effects.

Analytical models for thermo-structural failure during fire have been reported in the literature. Models based on buckling behavior have been proposed [7,20,21] with

limited validation. Suzuki *et al.* [11] developed empirical correlations to predict failure temperatures of beams and columns, but was limited to validation with data from fire resistance tests. Kandare *et al*. [15,16] evaluated use of creep-based failure models to predict failure times of small-scale compression tests on aluminum plates. Detailed finite element analysis was performed by Feih *et al.* [14] that show that creep effects are dominate at lower stresses and long exposure times.

No parametric study exists in the literature to systematically vary the important parameters controlling aluminum compression failure during realistic fire conditions. As a result, an experimental study was performed on an intermediate scale to investigate the effects of geometry, aluminum type, fire exposure severity, load, and fire protection on failure of aluminum during fire. The parametric evaluation of all of these parameters at this scale allows a comparison of these effects on failure, which is currently not possible with the existing literature data. The data was also used to develop and validate an empirical model for predicting aluminum failure that accounts for all of the evaluated parameters.

EXPERIMENTAL

Apparatus

All experiments were conducted using an intermediate-scale apparatus capable of applying 200 kN of compression load while subjecting one side to a constant heat flux up to 50 kW/m^2. A detailed description of the fire structural test apparatus and testing methodology is provided elsewhere [22]. As shown in Figure 1, the apparatus is composed of a compression loading frame, hydraulic loading system, heater assembly, instrumentation, and a sample.

The 2.29 m high, 1.22 m wide loading frame is constructed of steel box beam. At the bottom of the assembly there are three hydraulic jacks that are bolted to a stainless steel loading I-beam with a 0.15 m flange, 0.14 m web and a length of 0.95 m. An identical I-beam is also located at the top. Mounted to the top and bottom beams are clamps to produce fixed-fixed end conditions on the sample. This was experimentally validated through room temperature buckling tests [22].

The aluminum sample was placed in the loading frame clamps and secured at the ends by thread rods with 75 mm high, 100 mm wide faceplates as shown in the inset to Figure 1. To ensure a consistent boundary condition, a 13.56 N-m torque was applied to each rod. Heat loss from the sample to the mounting clamps was minimized by placing 12.7 mm thick Pyrotek NAD-11 insulation board between the clamp and sample. Clamps were thermally protected from the heaters using 25 mm thick ceramic fiber insulation blanket.

The hydraulic jack pressure was set to provide the desired load onto the sample. Tests were performed with a constant compression load applied to the plates by maintaining constant pressure to the hydraulic jacks. This was accomplished using a automatic bleed-off valve that ensured that the fluid pressure remained constant during the test, even when the sample experienced in plane deflections due to thermal expansion or out-of-plane bending. The applied load was directly measured using a series of Omega LCCA-15K load cells, each with a range of 0 to 66.7 kN and an accuracy of 0.037% of the full-scale range.

The electric heater panel assembly included three quartz-faced heater panels aligned vertically with total dimensions of 0.91 m in height and 0.30 m in width. Panel temperatures were controlled to provide a constant heat flux during the experiments. A shutter was used to shield the sample from heat exposure prior to test start time. Heat flux incident onto the sample was measured using a Medtherm #64-20SB-19 (Serial #158431) Schmidt-Boelter type, water-cooled total heat flux gauge with a range of 0 to 200 kW/m^2 and an accuracy of 3% of the full-scale range.

Sample temperatures and deflections were measured in the center of the sample at different locations along the height as shown in Figure 2. Temperatures were measured at seven locations along the height using 24 gauge, Type K bare bead thermocouples placed in the pilot hole drilled nearly through the sample. The thermocouple was then bonded and taped to the unexposed side of the sample with high temperature tape to reduce heat losses from the thermocouple (see Figure 1). In and out-of-plane deflections were measured using string potentiometers.

Materials

The experimental study included Al 5083-H116 and 6082-T651 aluminum alloy rolled plates, which are typically used in marine and other exterior applications. Aluminum alloy 5083-H116 is a strain hardened material while 6082-T651 is a temperature hardened alloy. In select tests, 5083-H116 samples were covered with 12.7 mm thick Superwool 607 fire insulation blanket with a density of 96 kg/m^3. Insulation was held against the surface using wire wrapped around the sample or using ten steel insulation pins tack welded to the aluminum surface. An overview of the samples used in the study is provided in Table 1. All plates were tested with the length of the sample being parallel to the rolling direction of the plate. Due to the rolling process, panels were measured to have some curvature with the center of the panel being 1.0-2.0 mm out of plane relative to the sample ends.

The stress-strain curves for these aluminum alloys at different temperatures are provided in Figure 3. The stress-strain curves for 6082-T651 are taken from Ref. [6]. The serrated yielding, also known as the Portevin-Le Chatelier (PLC) instability, is observed in Figure 3a for the 5083-H116 in the plastic region of the curve at 20^{o}C but is not evident at higher temperatures. For this aluminum alloy, the serrated yielding is attributed to the breaking away of mobile dislocations and Mg solutes [27]. As the temperature increases, the Mg solutes precipitate out of the solid solution allowing for dislocations to migrate more easily [27]. As expected, the elastic modulus and yield stress decrease with increasing temperature. For the 5083-H116 material shown in Figure 3a, the curves are nearly elastic-plastic behavior at all temperatures. The percent elongation at failure decreases from the room temperature value of 12% to a value of 2.5% at 180^{o}C. At higher temperatures (220-350^{o}C), the percent elongation at failure is higher and more constant (16.8-17.6%). The 6082-T651 material data [6] also displays elastic-plastic softening with increasing temperature (see Figure 3b), albeit with a consistent percent elongation at failure ranging from 12-14.5%.

Figures 4 and 5 contain plots of the modulus of elasticity and 0.2%-offset yield stress at elevated temperature for the two materials. The data in Figure 5 for 6082-T651

are from Refs. [6, 18]. The lines in the plots are a curve fit to the data based on the following form

$$B = \frac{B_{RT}}{2} - \frac{B_{RT}}{2}\tanh\left[k\left(T - T_{50\%}\right)\right] \quad (1)$$

where B is the elevated temperature property, B_{RT} is the property value at room temperature, T is the temperature, $T_{50\%}$ is the temperature where there is a 50% decrease in properties, and k defines the breadth of the curve. The appropriate constants for the each property are given in the plots. The 6082-T651 alloy has a higher modulus and yield stress at elevated temperature compared with the 5083-H116.

Test Conditions

A total of 62 experiments were conducted to evaluate the effects of a range of variables on the failure of aluminum plates during a fire exposure as well as room temperature failure tests. Parameters considered in the study included aluminum type, insulation, sample geometry (i.e., thickness, width, height), applied load, and heat flux. The aluminum type, insulation detail, geometric conditions tested and elevated temperature test conditions are outlined in Table 1. The majority of samples were exposed to three different heat fluxes (8, 19, and 38 kW/m^2) and subjected to loads that ranged from 10-85% of the room temperature Euler buckling load (provided in Table 1). A constant heat flux was used in the testing instead of the standard furnace time temperature curve. This was done to allow a more controlled study of the effects of different heat levels on the sample structural response.

The heat flux was applied to the surface of the sample over the entire height and width between the end clamps. Heat fluxes of 8, 19, and 38 kW/m^2 were measured at the center of sample. Closer to the edges of the sample, the heat flux decreases but remains within 20% of the center value. With heat fluxes of 8, 19, and 38 kW/m^2, the aluminum reached maximum temperatures of 225, 370 and 480^{o}C, respectively. Both the time-to-failure and the temperature at failure were used to evaluate the effect of these parameters on aluminum failure during fire exposure. All uninsulated samples were tested with the exposed surface painted black and the unexposed side unpainted in order to maximize the

sample temperature. The unexposed side of the sample was exposed to laboratory conditions.

RESULTS

Heat Flux and Applied Stress

The effect of heat flux and applied compressive stress on the time to failure is provided in Figure 6 for uninsulated 5083-H116 with a 0.737 m height, 0.203 m width, and various thicknesses. The normalized stress values are defined by the compressive stress applied to the aluminum panel when exposed to the heat flux divided by its original buckling stress at 20^{o}C. As expected, increasing the heat flux decreases the failure time at a given applied load. Similarly, increasing the applied load also decreases the time-to-failure. The lowest and intermediate heat fluxes show a minimum load required for failure in the defined 3600 second test period. At 8 kW/m^2, the minimum load is approximately 50% of the room temperature buckling load while at 19 kW/m^2 the minimum load is approximately 10% the room temperature buckling load. Applied loads less than the minimum were not capable of causing failure.

Geometry

Effects of sample geometry on the time-to-failure are provided in Figures 6 and 7. Figure 6 shows data for the effect of heat flux on the response of aluminum with three different thicknesses, while Figure 7 provides the effects decreasing width and height while keeping the heat flux constant at 19 kW/m^2. From data in Figure 6, the effect of thickness is mostly removed by normalizing the data with respect to the room temperature buckling load. Thicker samples did tend to fail at longer times, which may be expected due to the additional energy required to heat the thicker samples. However, the difference was within the 15% repeatability error of the failure times. As shown in Figure 7, effects of height and width of samples were also removed when normalizing the data with respect to the room temperature buckling load.

Aluminum Type

The structural survivability of the plates during fire testing was dependent on the type of aluminum alloy. A plot of the failure times for the two alloys for different heat

fluxes and applied stresses is given in Figure 8. The 6082-T651 alloy was measured to have longer times to failure. In addition, the minimum load levels at each heat flux required for failure was higher compared to those measured for the 5083-H116. At 8 kW/m^2, the minimum required failure load was 75% the buckling load for 6082-T651 while it was 50% for 5083-H116. The 6082-T651 alloy at 19 kW/m^2 had a minimum failure load of at least 25% which is again higher than the 10% value for 5083-H116. The trends in the results agree with the elevated temperature property data in Figures 4 and 5 where the modulus of the 6082-T651 is higher at elevated temperatures compared with the data for 5083-H116.

Failure Temperature

The constant heat flux levels applied during the tests resulted in the transient temperature profiles provided in Figure 9. As seen in the figure, increasing the heat flux results in more rapid temperature increase and higher temperatures after long exposure times.

The temperature of the plate at the mid-height at failure is plotted in Figure 10 against the normalized applied load for all of the tests on the 5083-H116 and 6082-T651 alloys without insulation. As seen in the figure, the temperature at failure decreases as the applied load increases. This data indicates that once the mechanical properties have sufficiently decreased by the increase in temperature, the plate is expected to fail.

Temperatures for failure range from 100 – 480^oC over applied stress levels between 10% and 80% of the room temperature buckling load. Failure temperatures in other small, intermediate, and large scale studies [6-10,11,14] were measured to range from 170-450^oC, which is a slightly smaller range compared to that measured here. This is attributed to the more narrow range of applied stress levels used in other studies as well as aluminum type. As previously mentioned, there is a distinct difference in failure temperature for the 5083-H116 and the 6082-T651 alloys which is in part attributed to the difference in elastic modulus. The deviations in failure temperature at particular normalized stress levels appear to be have a small dependence on applied heat flux, with higher heat fluxes resulting in higher failure temperatures. This may be due to creep effects. Creep would tend to cause the lower heat flux, longer duration tests to fail at lower temperatures than the higher heat flux, shorter duration tests.

Fire Insulation

Failure time and temperature at failure for tests with fire insulation on the aluminum surface are provided in Figure 11. All insulated tests were conducted with an incident heat flux of 38k W/m^2 using 7.35 mm thick, 0.737 m high, 0.23 m wide 5083-H116 samples. The data is plotted with results from uninsulated 5083-H116 aluminum samples having the same size and thickness as the insulated aluminum plate.

The time-to-failure of the insulated samples shown in Figure 11a were longer than those measured for uninsulated plates exposed to 8 kW/m^2. A significant temperature drop exists through the insulation (400-500^{o}C) which reduces the heat transfer to the aluminum sample. Based on the thermal properties of the insulation, the heat flux into the aluminum was predicted to be 4-6 kW/m^2 during the exposure. This result justifies the longer failure times for the insulated samples compared with the uninsulated samples at 8 kW/m^2. In these tests, no difference was measured for cases where the insulation was attached with wire or pins.

The failure temperatures for the insulated and uninsulated samples are provided in Figure 11b. Despite differences in times to failure, the temperatures at which the insulated and uninsulated samples failed were similar and followed the same trend with applied load.

DISCUSSION

Failure Temperature Criterion

The basis for structural failure criteria for aluminum alloys during fire exposure is typically based on a single temperature criterion, which varies depending on the application. These criteria are largely based on an ad-hoc assessment of when the strength decreases by a certain fraction from the room temperature value. Most regulatory agencies (International Maritime Organization (IMO) in the High Speed Craft Code and U.S. Coast Guard) require that protection be sufficient to prevent the aluminum from exceeding 230^{o}C during a standard fire resistance test [23]. Other marine applications require that the aluminum temperature cannot rise by more than 200^{o}C [24]. These failure criteria are based on the temperature at which aluminum alloys typically lose half their room temperature strength [19]. Kaufman and Kasser [25] also suggested

that the failure temperature be between a temperature that a) ensures yield strength equal to the design allowable stress (~260^{o}C) or b) ensures there will be no substantial change in room temperature properties due to heating (190^{o}C). The Eurocode 9: Part 1-2 [18] for design of aluminum structures against fires recommends a failure temperature of 170^{o}C. Maljaars *et al.* [9] measured critical failure temperatures ranging from 170-375^{o}C in tension tests at various constant heating rates (1.6-11^{o}C/min). The failure temperature was dependent on the applied stress level. Suzuki et al. [11] also measured a range of critical temperatures (250-450^{o}C) for aluminum in compression tests that was dependent on aluminum alloy type, applied stress, and slenderness ratio.

The failure temperatures in the intermediate-scale compression tests on aluminum 5083-H116 and 6082-T651 with constant heat flux fire exposures are shown in Figure 9 to range from 100-480^{o}C, and was determined to be a function of applied stress level. Clearly, a single temperature failure criterion for all parts of the structure may lead to excessive protection or possibly insufficient protection, depending on the stress variations within the design as well as load redistributions due to partial structural failure. Such failure criteria still need to be investigated for other loading conditions, aluminum types, and additional structural detail. Due to the sensitivity of the failure temperature to applied stress, fire resistance tests that include structural load are a more reliable method for evaluating structural integrity during fire rather than a single temperature criterion.

Analysis of Compression Failure

Results presented in the previous section demonstrated that the compression failure of aluminum is dependent on applied stress, temperature, material type and panel geometry. For a single type of aluminum, a correlation is shown in Figure 10 to exist between failure temperature and applied stress. However, change in aluminum type results in a different correlation. Analysis was performed to develop an approach for predicting failure of different types of aluminum during fire. The method is based on the approach developed by Mazzolani [5] for correlating failure of different types of aluminum at room temperature. This method was modified to include the effects of elevated temperature on the mechanical properties.

The failure model developed here considers both buckling failure and yield stress as the two failure modes. Through this method, failure is predicted when either the yield

stress or buckling stress is exceeded. Consideration of these two stresses is required because failure of short samples (small slenderness ratios) is controlled by the yield stress of the material while longer samples (larger slenderness ratios) will fail due to physical buckling of the specimen. The effect of temperature dependence on the failure is included by developing slenderness ratios and failure stresses that are nondimensionalized with respect to elevated temperature properties. Stress-strain curves are assumed to behave as elastic-plastic. This is reasonable based on the stress-strain curves in Figure 3 and the failure temperatures.

The nondimensional slenderness ratio is defined as

$$\Lambda = \frac{\lambda}{\lambda_o} \tag{2}$$

which is the slenderness ratio, λ, divided by the critical slenderness ratio, λ_o. The slenderness ratio is defined as

$$\lambda = \frac{L_e}{r} \tag{3}$$

where the effective length, L_e, is half of the exposed length for fixed-fixed boundary conditions and the radius of gyration for a plate of rectangular cross-section is

$$r = \frac{t}{\sqrt{12}} \tag{4}$$

where t is the plate thickness. The critical slenderness ratio is the slenderness ratio at which the failure mechanism transitions from yield stress failure to buckling failure. The critical slenderness ratio was determined by setting the 0.2% offset yield stress equal to the Euler buckling stress,

$$\lambda_o = \pi\sqrt{\frac{E}{\sigma_{0.2}}} \tag{5}$$

where the modulus of elasticity, E, and the 0.2% offset yield stress, $\sigma_{0.2}$, are properties at elevated temperature. The nondimensionalized stress was determined as

$$N = \frac{\sigma}{\sigma_{0.2}} \tag{6}$$

where σ is the applied stress and 0.2% offset yield stress, $\sigma_{0.2}$, is the property at elevated temperature.

The proposed approach for predicting failure would be to determine whether a sample fails due to yielding or buckling. At a particular dimensionless slenderness ratio, the normalized failure stress is defined as

$$N_f = \frac{\sigma_f}{\sigma_{0.2}} \tag{7}$$

where the value of yield stress, $\sigma_{0.2}$, is evaluated at the sample temperature. The failure stress, σ_f, is the lower of the yield stress at the sample temperature or the Euler buckling stress,

$$\sigma_B = \frac{\pi^2 E}{\lambda^2} \tag{8}$$

determined using the modulus at the sample temperature.

Equations (7) and (8) were used to develop the failure plot shown in Figure 12. This failure curve accounts for the effects of elevated temperature on the mechanical properties in both the yield and buckling regimes. In addition, it is similar in shape to the failure curve proposed by Mazzolani [5] for correlating room temperature failure of different materials that this development was based upon. Elevated temperature properties were determined using Equation 1 and the constants given in Figures 4 and 5. Failure is predicted when the nondimensional stress and slenderness ratio result in a point that is above the failure curve. Due to using yield stress and modulus at elevated temperature, the failure curve shown in Figure 12 is valid for all temperatures. Based on this model, nondimensional slenderness ratios of less than 1.0 will fail due to yield stress while higher values will fail due to buckling.

The data shown in Figure 12 is from the compression failure tests of the 5083-H116 and 6082-T651 plates. Properties for the nondimensional parameters were evaluated at the failure temperature. As seen in the figure, all of the cases tested in the

intermediate scale tests are within the region where failure is expected due to buckling except for one of the 6082-T651 cases. The percent difference between all the data and the failure curve is 25% and the samples generally fail before expected through the failure curve criteria. This earlier than expected failure is attributed to samples not being perfectly flat and creep effects. Creep effects in aluminum will become significant when temperatures exceed approximately 200^{o}C. Samples with failure temperatures exceeding 200^{o}C and long exposure durations are expected to have more significant creep effects [14-16]. Despite not accounting for these effects, the model does quite well at predicting the failure for different materials under different loads and exposure conditions.

A statistical analysis of the data was performed to determine a multiplying factor that would need to be applied to the stress in Equation (6) to result in a conservative correlation of the data with the failure curve. It was determined that a multiplier of 1.6 on the applied stress provided a conservative correlation of the data relative to the failure curve.

The compression failure model shown in Figure 12 can be used in multiple ways. In general, the model is dependent on sample temperature, applied stress and sample slenderness ratio (i.e., geometry). If any two of these parameters are selected, then the acceptable range for the remaining parameter may be identified. For example, if the applied stress is known and the geometry is given then the maximum operating temperature can be determined. The model does require knowledge of the elastic modulus and 0.2% offset yield stress as a function of temperature. The approach presented above provides a simple analytical estimate of the possibility for failure; however, the inclusion of creep effects is required for more accurate assessment of the response.

CONCLUSIONS

An experimental study was performed to quantify the response and failure of aluminum plates under compression load while being subjected to a constant heat flux representing a fire exposure. The effect of plate geometry (thickness, height, width) on failure was accounted for through normalizing applied stress with the room temperature Euler buckling stress. With the addition of fire insulation, the heat flux into the plate was

reduced but the failure behavior was similar to that observed in lower heat flux tests without insulation. Failure temperatures were measured to range from 100-480^{o}C and were dependent on applied stress and aluminum type. Due to the sensitivity of the failure temperature to applied stress, fire resistance tests that include structural load are a more reliable method for evaluating structural integrity during fire rather than conducting fire resistance tests without loading and using a single temperature criterion. An empirical failure model was developed to account for fire exposure conditions, aluminum type, and geometry. The simple analytical model was able to predict the occurrence of failure to within 25% without including the effects of creep and initial flatness imperfection. The inclusion of creep effects is required for more accurate assessment of the response.

ACKNOWLEDGEMENTS

The authors appreciate the funding for this research provided by the Office of Naval Research through Grant No. N00014-08-1-0528.

REFERENCES

1. Mofflin, D. and Dwight, J., 1983, "Tests on Individual Aluminum Plates Under In-Plane Compression," Report CUED/D-STRUCT/TR-100, Cambridge University, 77p.
2. Hopperstad, O., Langseth, M., and Hanssen, L., 1998, "Ultimate Compressive Strength of Plate Elements in Aluminum : Correlation of Finite Element Analyses and Tests," *Thin-Walled Structures*, Vol. 29, Nos. 1-4, pp.31-36.
3. Zha, Y. and Moan, T., 2003, "Experimental and Numerical Prediction of Collapse of Flatbar Stiffeners in Aluminum Panels," *Journal of Structural Engineering*, Vol. 129, No.2, pp.160-168.
4. Paik, J. and Duran, A., 2004, "Ultimate Strength of Aluminum Plates and Stiffened Panels for Marine Applications," *Marine Technology*, Vol. 41, No.3, pp.108-121.
5. Mazzolani, F., 1995, Aluminum Alloy Structures, 2nd Edition, Chapman & Hall.
6. Langhelle, N., Eberg, E., Amdahl, J., and Lundberg, S., 1996, "Buckling Tests of Aluminum Columns at Elevated Temperatures," 1996 OMAE – Volume II Safety and Reliability, pp.387-394.

7. Maljaars, J., Soetens, F., and Snijder, H., 2009, “Local Buckling of Aluminum Structures Exposed to Fire. Part 1:Tests,” *Thin-Walled Structures*, Vol. 47, pp.1404-1417.
8. Maljaars, J., Twilt, L., and Soetens, F., 2009, “Flexural Buckling of Fire Exposed Aluminum Columns,” *Fire Safety Journal*, Vol. 44, pp.711-717.
9. Maljaars, J., Soetens, F., and Katgerman, L., 2008, “Constitutive Model for Aluminum Alloys Exposed to Fire Conditions,” *Metallurgical and Materials Transactions A*, Vol.39A, pp.778-789.
10. Amdahl, J., Langhelle, N., and Lundberg, S., 2001, “Aluminum Plated Structures at Elevated Temperatures,” Proceedings of OMAE 2001, pp.309-316.
11. Suzuki, J., Ohmiya, Y., Wakamatsu, T., Harada, K., Yuasa, S., and Kohno, M., 2005, “Evaluation of Fire Resistance of Aluminum Alloy Members,” Fire Science and Technology,” Vol. 24, pp.237-255.
12. Parker, W.J., 1972, “Fire Endurance Tests of Aluminum Bulkhead and Deck Assemblies,” National Bureau of Standards, Report No. 10813.
13. Bausano, J., Lesko, J., and Case, S., 2007, “The Comparison of the Response of 6061 Aluminum and Glass/VE Composite to Simulated Fire Exposure Conditions,” Proceedings of the 4th Composites and Fire Conference.
14. Feih, S., Kandare, E., Lattimer, B.Y., and Mouritz, A.P., “Structural Analysis of Compression Deformation and Failure of Aluminum in Fire,” *Journal of Structural Engineering*, http://dx.doi.org/10.1061/(ASCE)ST.1943-541X.0000313, 2010.
15. Kandare, E., Feih, S. Lattimer, B.Y., Mouritz, A.P., “Larson-Miller Failure Modelling of Aluminum in Fire,” Metallurgical and Materials Transactions A, Vol.41, No.12, pp.3091-3099, 2010.
16. Kandare, E., Feih, S., Lattimer, B.Y., and Mouritz, A.P., “Creep-Based Life Prediction Modelling of Aluminum in Fire,” *Journal of Materials Science*, Vol. 527, Issues 4-5, pp.1185-1193, 2010.
17. EN 1999:1-1, 2009, “Eurocode 9 - Design of Aluminum Structures – Part 1-1 : General Rules,” British Standard.
18. EN 1999-1-2:2007, 2009, “Eurocode 9 - Design of Aluminum Structures – Part 1-2 : Structural Fire Design,” British Standard.

19. Winer, A. and Butler, F., 1975, “Passive Fire Protection for Aluminum Structures,” *Naval Engineers Journal*, December, pp.59-66.
20. Maljaars, J., Soetens, F., and Snijder, H., 2009a, “Local Buckling of Aluminum Structures Exposed to Fire Part 2: Finite Element Models,” *Thin-Walled Structures*, Vol. 47, pp.1418-1428.
21. Knobloch, M. and Fontana, M., 2005, “Load-carrying Behavior of Unstiffened Elements at Elevated Temperatures in Fire,” *Fire Safety Science-Proceeding of the Eighth International Symposium*, pp.223-234.
22. Fogle, E. , “Compression Failure of Aluminum Plates Exposed to Constant Heat Flux,” Master’s Thesis, Virginia Polytechnic Institute and State University, 2010.
23. IMO Resolution A.754(18), 1998, “Recommendation on Fire Resistance Tests for “A”, “B” and “F” Class Division,” *FTP Code – International Code for Application of Fire Test Procedures*, International Maritime Organization, London.
24. Sorathia, U., 2007, “Fire Resistant Divisions in U.S. Naval Ships,” SAMPE 2007.
25. Kaufman, J. and Kasser, R., 1963, “Fire Protection for Aluminum Alloy Structural Shapes,” *Civil Engineering*, pp.46-47.
26. Kaufmann, J., “Properties of Aluminium Alloys – tensile, creep and fatigue data at high and low temperatures,” ASM International, 1999, ISBN 0-87170-632-6.
27. W. Wen and J.G. Morris, “An Investigation of Serrated Yielding in 5000 Series Aluminum Alloys,” *Materials Science and Engineering*, A354, 2003, pp. 279-285.

Table 1 Samples and test conditions evaluated tested in the study.

Sample No.	**Material (HxWxt) (mm)**	**Insulation**	**Buckling Load (kN)**	**Applied Heat Flux (kW/m^2)**	**Applied Load (%-buckling load)**
1	5083-H116 (737 x 203 x 6.35)	NO	23.8	8	51, 74, 79
				19	20, 52, 77
				38	22, 28, 31, 46
2	5083-H116 (737 x 203 x 7.94)	NO	46.4	8	42, 53, 64, 68
				19	12, 29, 38, 52, 75
				38	12, 25, 47, 51
3	5083-H116 (737 x 203 x 9.53)	NO	80.2	8	43, 51, 54, 63
				19	17, 23, 42
				38	12, 23, 43
4	5083-H116 (660 x 203 x 7.94)	NO	57.7	19	22, 42, 60
5	5083-H116 (737 x 102 x 7.94)	NO	23.2	19	22, 53, 61
6	5083-H116 (737 x 203 x 7.94)	YES[1]	46.4	38	48, 57, 69, 71, 72
7	6082-T6 (737 x 203 x 7.94	NO	43.1	8	69
				19	25, 49, 68
				38	12, 24, 47

[1]Fire insulation was 12.7 mm thick Superwool 607 with 96 kg/m^3 density

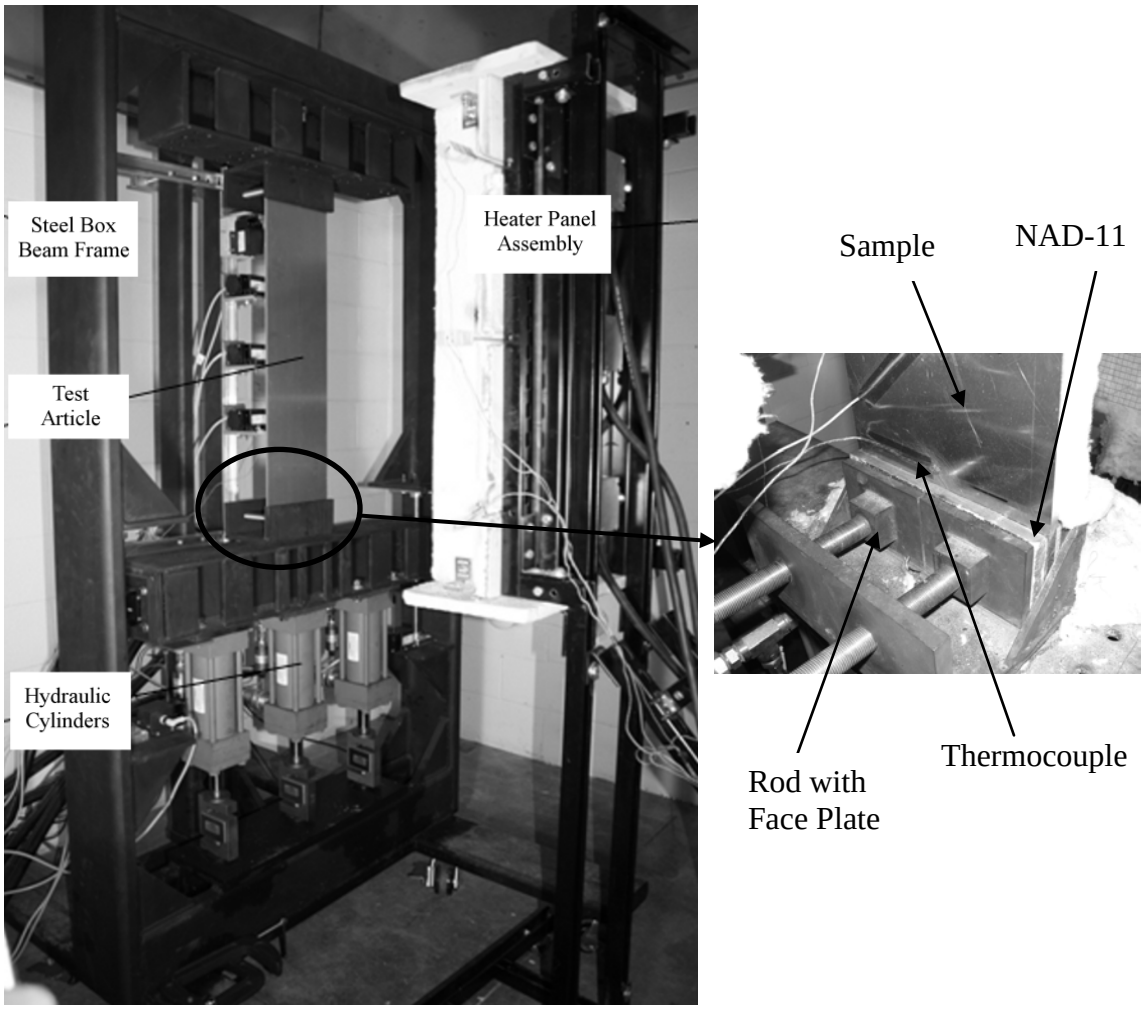

Figure 1. Compressive loading frame apparatus with clamp detail.

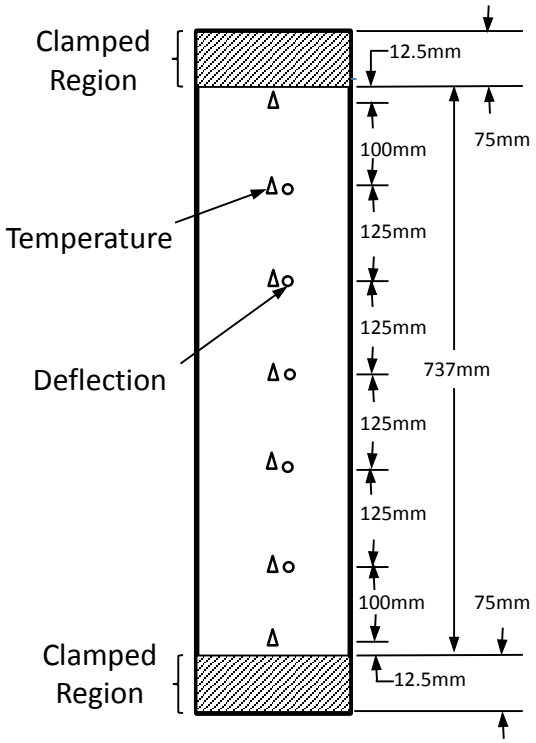

Figure 2. Location of thermocouple and deflection measurements on samples.

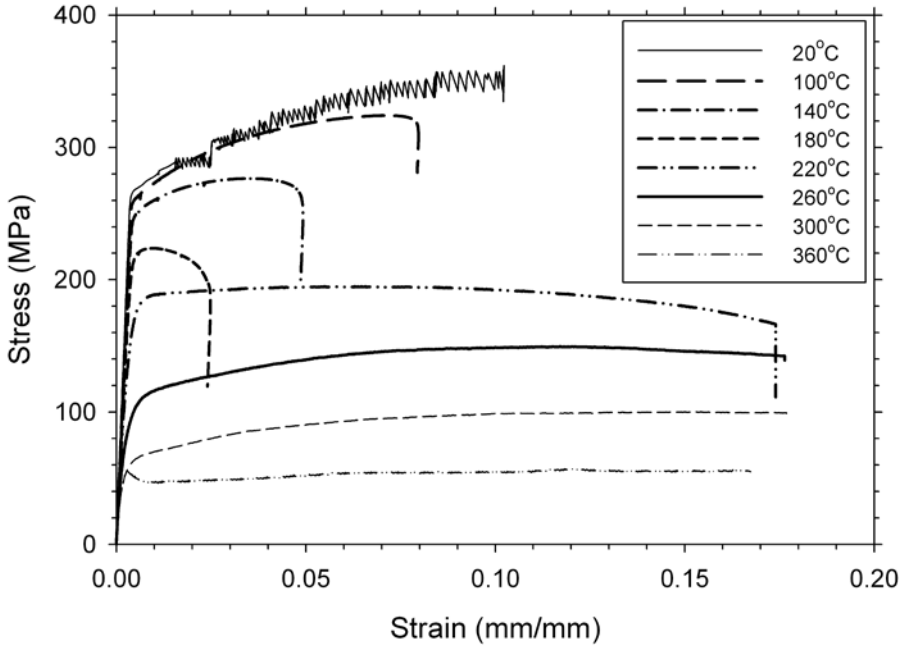

(a)

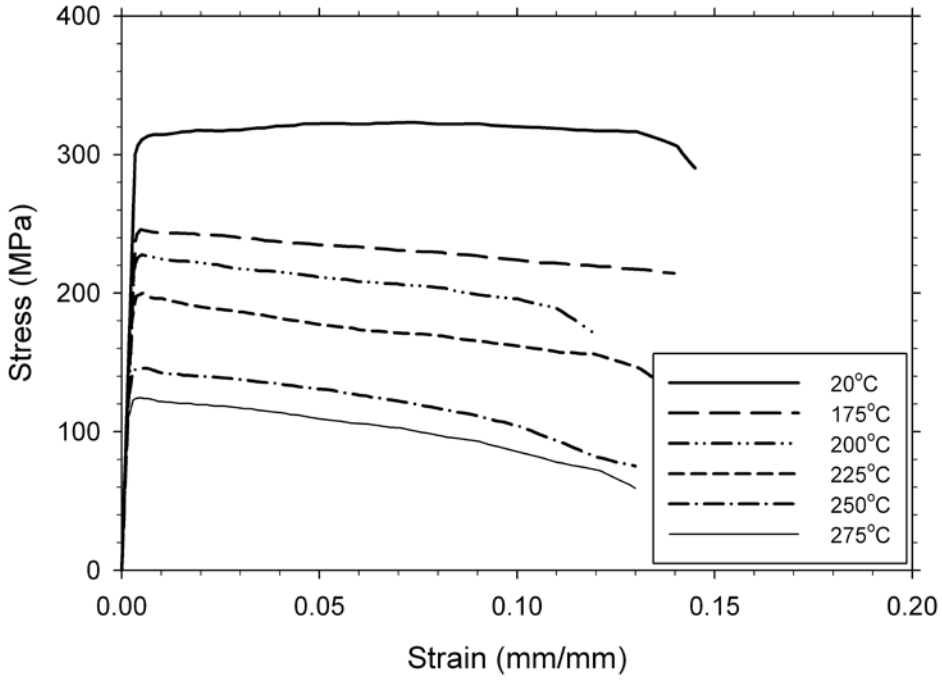

(b)

Figure 3. Elevated temperature stress-strain curves for a) 5083-H116 and b) 6082-T651 [6].

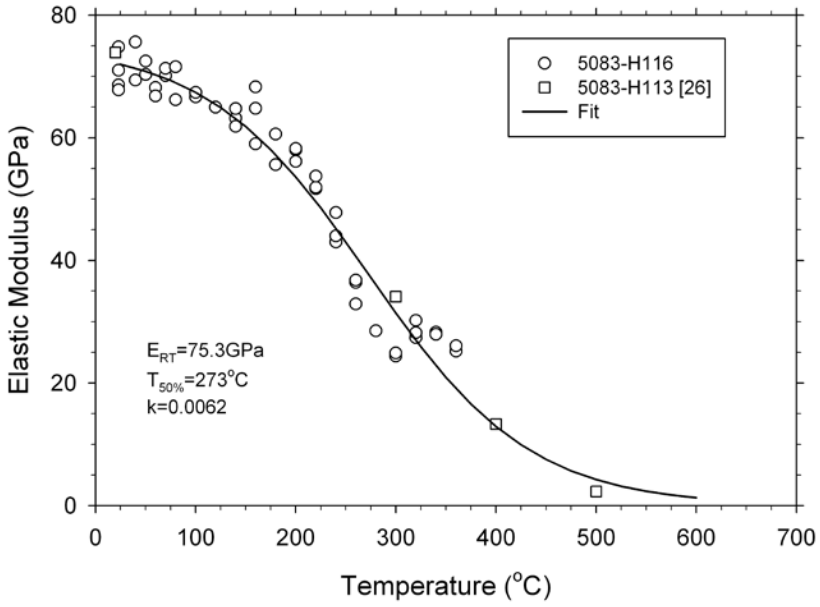

(a)

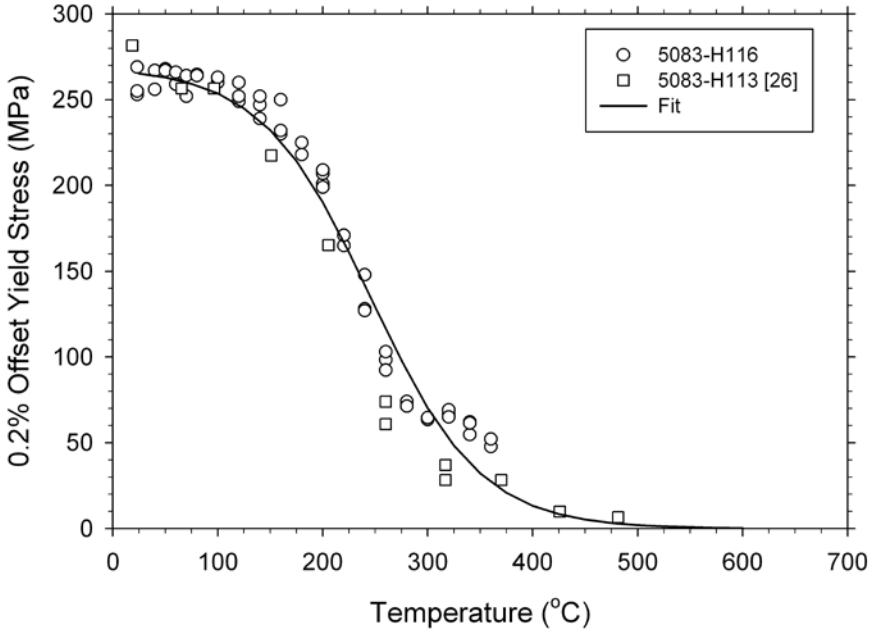

(b)

Figure 4. 5083-H116 elevated temperature a) elastic modulus and b) 0.2%-offset yield stress.

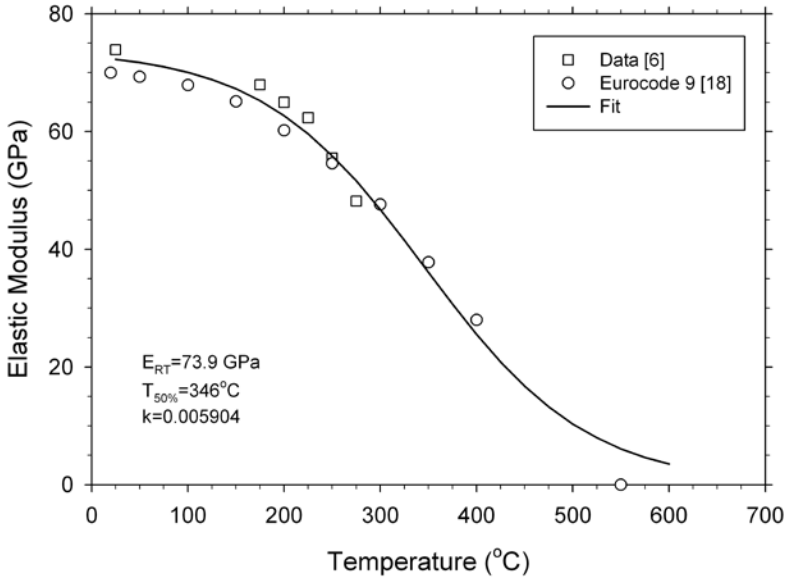

(a)

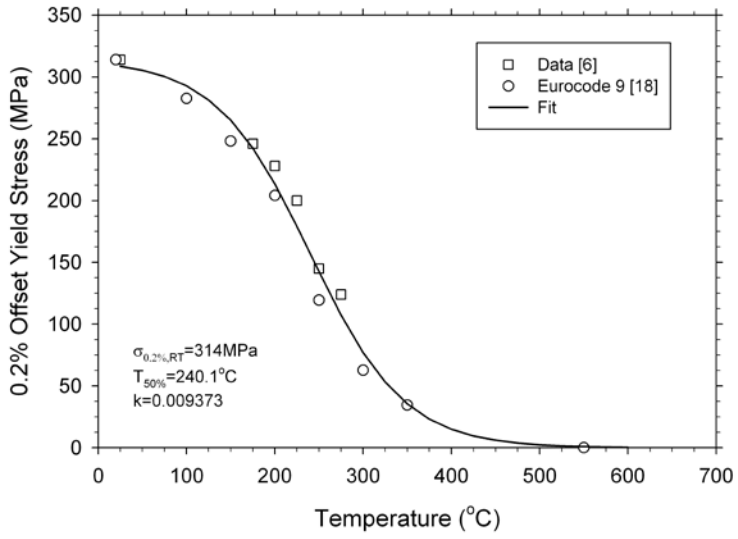

(b)

Figure 5. 6082-T651 elevated temperature a) elastic modulus and b) 0.2%-offset yield stress [6, 18].

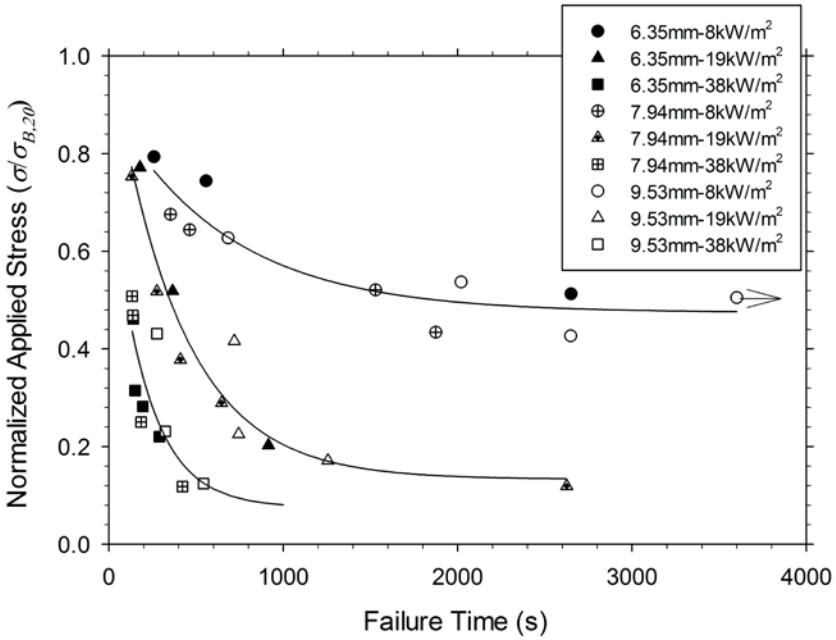

Figure 6. Effect of heat flux on failure of 5083 H116 for thicknesses of 6.35, 7.94, and 9.53 mm. Data point with arrow did not fail after 3600 sec. Lines represent data trends.

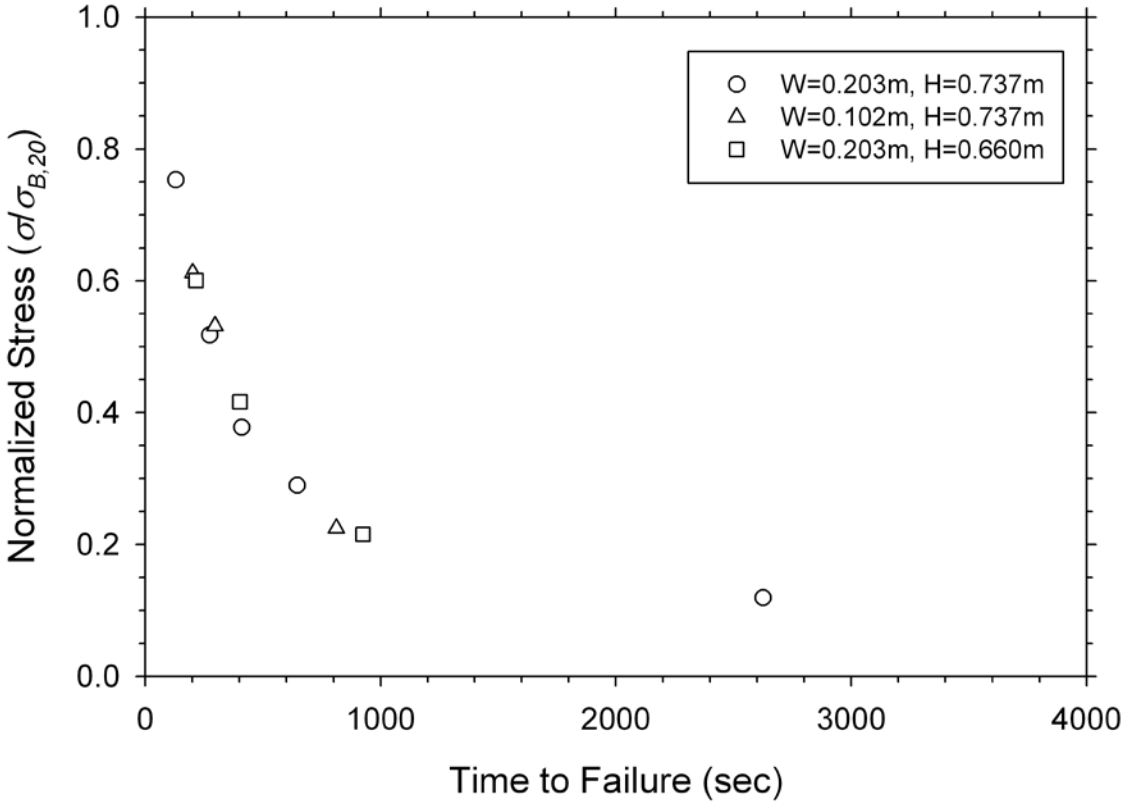

Figure 7. Effect of height and width on failure of 5083 H116, 7.94 mm thick at 19 kW/m^2.

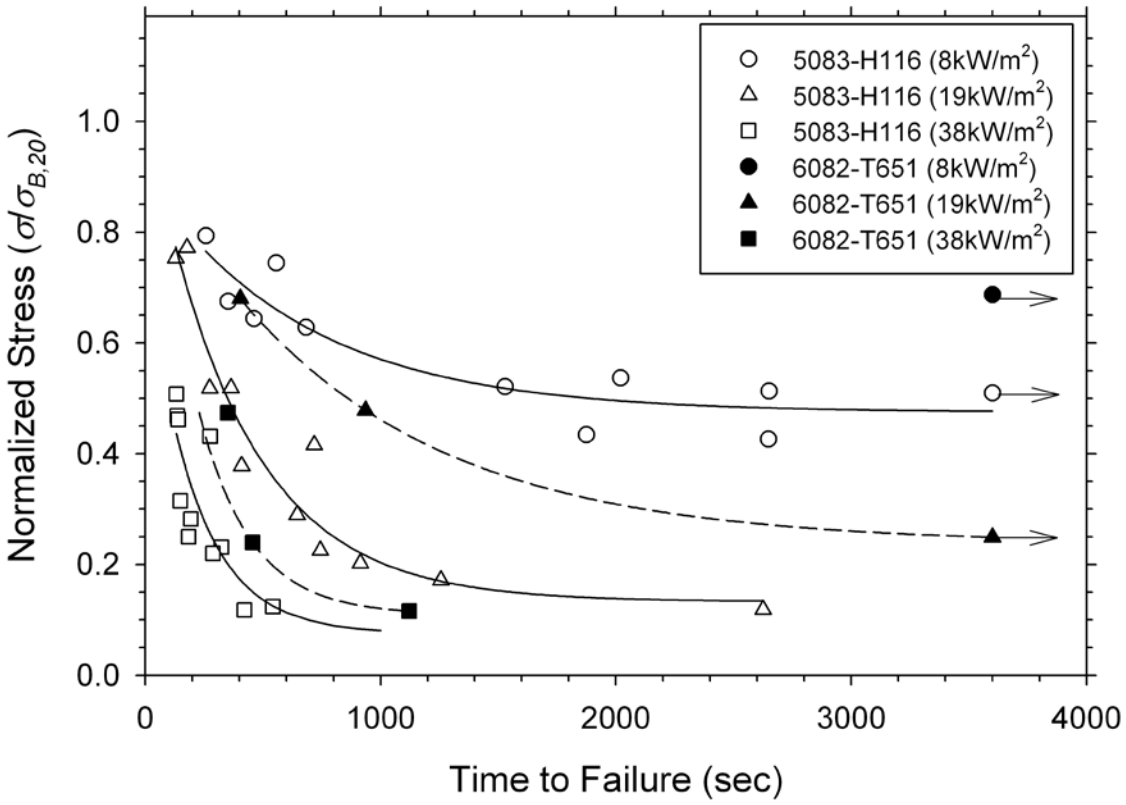

Figure 8. Failure times for different aluminum alloys. 5083-H116 tested at thicknesses of 6.35, 7.94, and 9.53 mm while 6082-T651 was 7.94 mm thick. Data points with arrow did not fail after 3600 sec. Lines represent data trends.

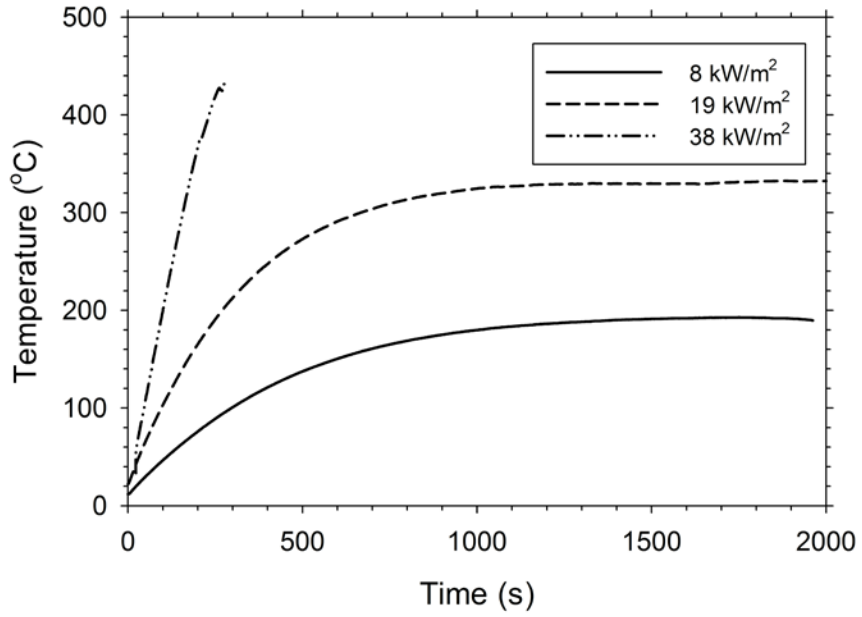

Figure 9. Temperature at the panel mid-height for different heat flux levels.

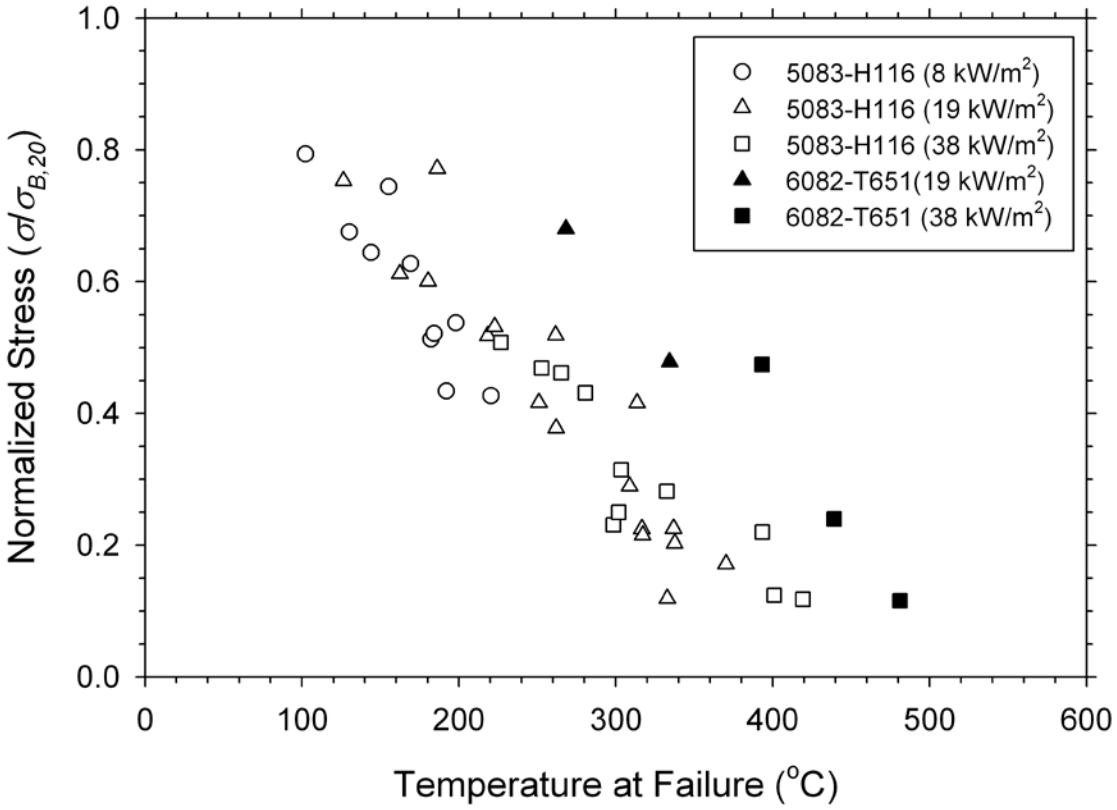

Figure 10. Effect of aluminum type on failure.

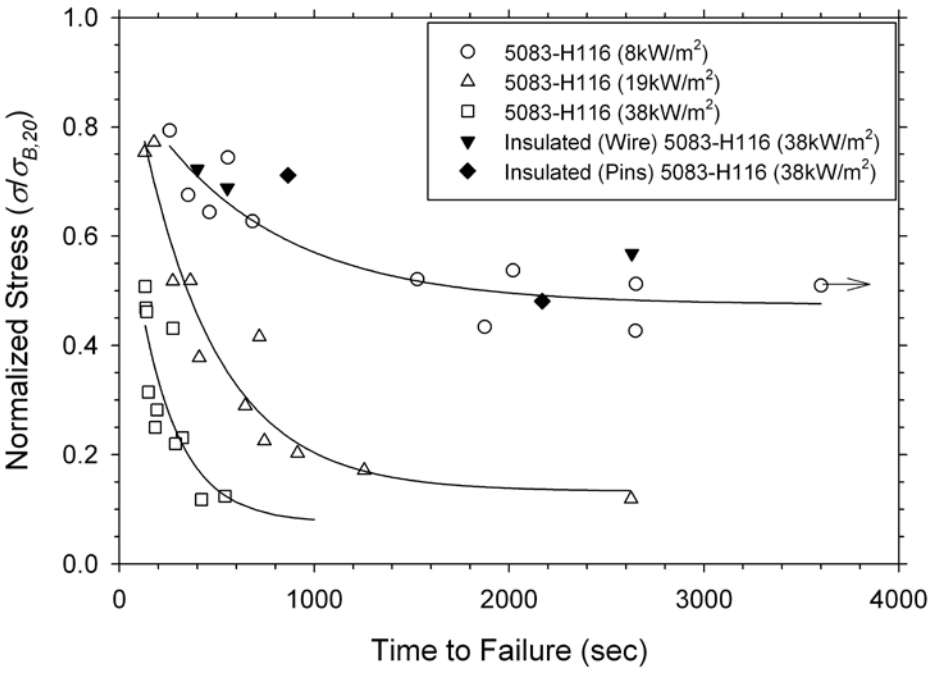

(a)

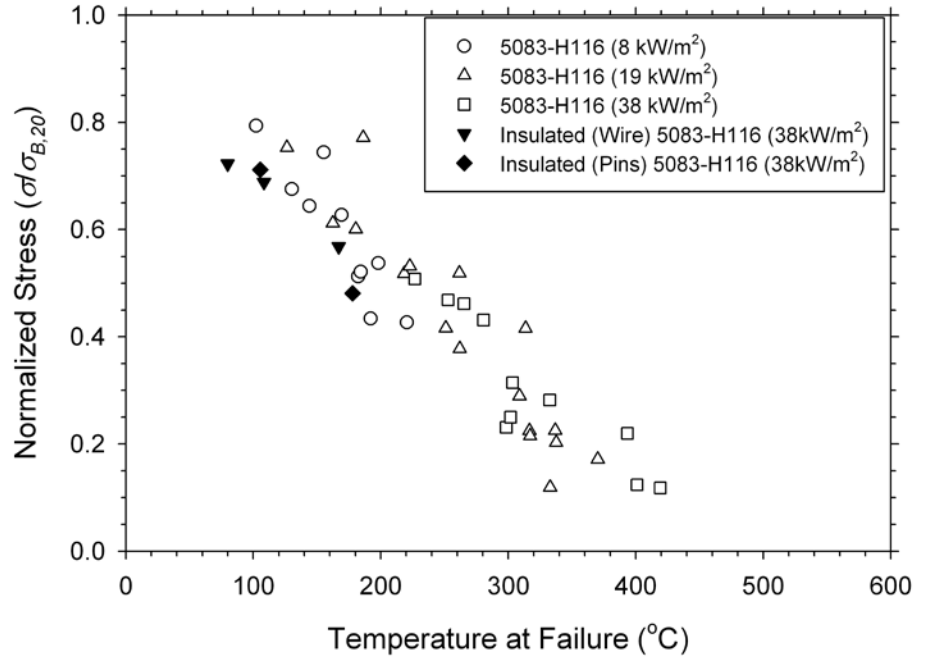

(b)

Figure 11. Effect of fire insulation on a) time-to-failure and b) temperature at failure. Data point with arrow did not fail after 3600 sec. Lines represent data trends.

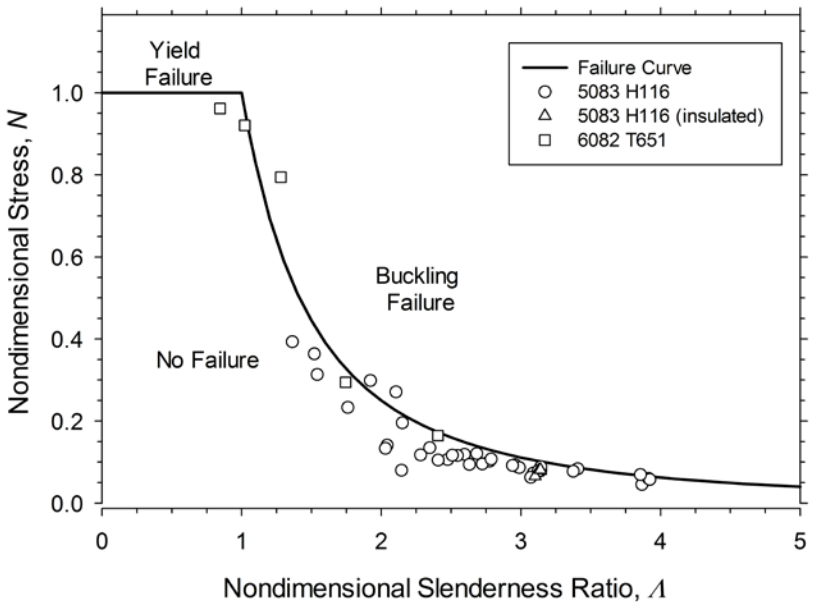

Figure 12. Failure plot including effect of temperature and slenderness ratio. Line represents failure curve.